Environmental Science & Technology

pubs.acs.org/est

Article

Laboratory Investigation of Renoxification from the Photolysis of Inorganic Particulate Nitrate

Qianwen Shi, Ye Tao, Jordan E. Krechmer, Colette L. Heald, Jennifer G. Murphy, Jesse H. Kroll, and Qing Ye*

Cite This: *Environ. Sci. Technol.* 2021, 55, 854–861

Read Online

ACCESS | Metrics & More | Article Recommendations | Supporting Information

ABSTRACT: Nitrogen oxides (NO_x) play a key role in regulating the oxidizing capacity of the atmosphere through controlling the abundance of O_3, OH, and other important gas and particle species. Some recent studies have suggested that particulate nitrate, which is conventionally considered as the ultimate oxidation product of NO_x, can undergo "renoxification" via photolysis, recycling NO_x and HONO back to the gas phase. However, there are large discrepancies in estimates of the importance of this channel, with reported renoxification rate constants spanning three orders of magnitude. In addition, previous laboratory studies derived the rate constant using bulk particle samples collected on substrates instead of suspended particles. In this work, we study renoxification of suspended submicron particulate sodium and ammonium nitrate through controlled laboratory photolysis experiments using an environmental chamber. We find that, under atmospherically relevant wavelengths and relative humidities, particulate inorganic nitrate releases NO_x and HONO less than 10 times as rapidly as gaseous nitric acid, putting our measurements on the low end of recently reported renoxification rate constants. To the extent that our laboratory conditions are representative of the real atmosphere, renoxification from the photolysis of inorganic particulate nitrate appears to play a limited role in contributing to the NO_x and OH budgets in remote environments. These results are based on simplified model systems; future studies should investigate renoxification of more complex aerosol mixtures that represent a broader spectrum of aerosol properties to better constrain the photolysis of ambient aerosols.

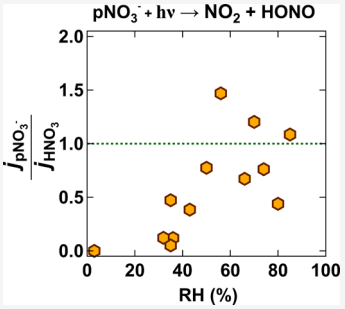

1. INTRODUCTION

Nitrogen oxides (NO_x = NO + NO_2) are key trace gases that regulate the chemistry and life cycles of many species in the atmosphere. The dominant sinks of NO_x include nitric acid (HNO_3), formed by NO_2 + OH and nitrogen pentoxide (N_2O_5) hydrolysis, and organic nitrates, formed by the oxidation of volatile organic compounds. HNO_3 can partition into particles or be generated in particles to form inorganic particulate nitrate, which is a globally important component of ambient particulate matter.[1] Traditionally, gaseous and particulate nitrate are considered to be the chemical end point of the NO_x life cycle in the atmosphere prior to wet or dry deposition. However, there has been growing interest in the potential importance of particulate nitrate renoxification in remote regions far from NO_x emissions. Renoxification, which typically involves the photolysis of nitrate on material surfaces[2−4] and in bulk solution,[5,6] is a process that directly converts nitrate back into NO_x or indirectly via nitrous acid (HONO), subsequently affecting the O_3 and OH budgets.

Photolysis of gaseous HNO_3 yields NO_x and HONO with a rate constant (j_{HNO_3}) on the order of 10^{-7} s^{-1} in the troposphere,[7] representing a minor sink of HNO_3. Photolysis of aqueous nitrate is also known to produce NO_2 and the nitrite ion (NO_2^-) in bulk solutions via the following reactions:

$$NO_3^-(aq) + H^+ + h\nu \rightarrow NO_2 + OH \quad (R1)$$

$$NO_3^-(aq) + h\nu \rightarrow NO_2^- + O(^3P) \quad (R2)$$

NO_2^- will form HONO that can partition into the gas phase[5,6,8] or undergo further photolysis forming NO. While NO and NO_2 are likely to escape to the gas phase, OH radicals produced in the bulk phase are more likely to react in the condensed phase. Within the atmospherically relevant wavelength range (> 290 nm), the absorption spectrum of aqueous nitrate peaks at ∼302 nm.[2] The effective quantum yields for wavelengths ≥290 nm for R1 is estimated to be ∼1%.[8] The reported quantum yield for R2 varies from a fraction of a percent to several percent, depending on the properties of the solution.[8]

Surface-adsorbed nitrate is understood to undergo more rapid photolysis compared to bulk aqueous nitrate, with a quantum yield as high as 0.8 at room temperature.[9] Studies of

Received: September 8, 2020
Revised: December 6, 2020
Accepted: December 7, 2020
Published: January 4, 2021

https://dx.doi.org/10.1021/acs.est.0c06049
Environ. Sci. Technol. 2021, 55, 854–861

nitrate photolysis on surfaces of snow and ice,[2] vegetation,[10,11] and other types of surfaces[12−15] usually find the photolysis rate constants to be between 10^{-5} and 10^{-3} s^{-1}, which are 2−4 orders of magnitude higher than j_{HNO_3}in the atmosphere.

Recently, some studies have proposed that photolysis of particulate nitrate can be an important *in situ* source of NO_x, as some ambient measurements reported higher than expected NO_x or HONO levels.[16,17] Several field, laboratory and modeling efforts have been carried out to quantify the renoxification rate constant via particulate nitrate photolysis and its impacts on NO_x and HONO budgets in the remote marine boundary layer,[16−19] in urban environments,[20−22] and in wildfire plumes.[23] It has also been suggested that in-particle production of OH and NO_2 from particulate nitrate photolysis plays a key role in in heterogeneously converting SO_2 to sulfate during haze events.[24−26] The derived photolysis rate constants from these studies are often expressed as nitrate photolysis enhancement factors with respect to j_{HNO_3} (hereinafter referred as the enhancement factor) shown in eq E1:

$$\text{enhancement factor} = \frac{j_{pNO_3^-}}{j_{HNO_3}} \quad \text{(E1)}$$

where $j_{pNO_3^-}$ is the first-order rate constant for NO_x or HONO formation from particulate nitrate photolysis. Currently, there is a wide range in reported enhancement factors, spanning three orders of magnitude. For example, using aircraft measurements over the North Atlantic Ocean, Ye *et al.* suggested that the enhancement factor can be as large as 300, indicating that particulate nitrate photolysis is an important *in situ* source of NO_x.[16,21] However, Romer *et al.* found that small to moderate enhancement factors (1−30) are the most consistent with aircraft observations over the Yellow Sea.[18] The divergent results from several studies hinder a consensus on the importance of renoxification from particulate nitrate photolysis on tropospheric chemistry, especially in regions far from NO_x emissions.

Laboratory experiments are crucial tools for studying the renoxification of particulate nitrate as they provide detailed and controlled evaluation of the kinetics and products of the photolysis process. While a handful of laboratory studies have shown substantial renoxification from condensed-phase nitrate,[6,8,25,27] experiments have been carried out using light sources that were not well-described or covered only a single wavelength (usually 310 nm or lower), leading to ambiguities as to how well the experiments mimic atmospheric conditions. In addition, previous studies photolyzed bulk particle samples that were collected on substrates in which the change of particle water content, evaporation of semi-volatile species, and substrate interferences can complicate extrapolations to real atmospheric particles. For example, the enhancement factor derived in Ye *et al.*[16] was consistent with some ambient measurements,[21] but was found to overestimate HONO productions from particulate nitrate photolysis in aged wildfire plumes.[23] This highlights the challenge of unraveling the effects of various complex particulate systems on nitrate renoxification.

In this work, we present results from laboratory photolysis experiments on inorganic particulate nitrate to quantify the first-order rate constants for renoxification using suspended particles in an environmental chamber with well-characterized light conditions. We focus on sodium nitrate and ammonium nitrate particles as our model systems. We explore the effects of wavelength, relative humidity (RH), and the presence of photosensitizers.

2. MATERIALS AND METHODS

2.1. Experimental Setup and Instruments. The experiments were conducted in a 150 L Teflon chamber run in semi-batch mode.[28] The chamber (shown in Figure S1) was filled with ultra-zero air (Airgas) during experiments, and a total flow of 6−8 lpm of ultra-zero gas was injected continuously into the chamber during each experiment. The mixing time was ≤1 min inside the chamber, and the residence time was 19−25 min. Ultraviolet lamps (18 40 W UVA or UVB fluorescent lights, Q-lab Corp.) surrounded the chamber; the characterization of the lamp output is described in Section 2.3.

Experiments focused on three model systems: sodium nitrate, ammonium nitrate, and sodium nitrate with added photosensitizers (imidazole, IM, >99.5%, 2-imidazolecarboxaldehyde, IM-CHO, 97%, and pyruvic acid, PA, 98%, Sigma-Aldrich). Imidazoles have been detected in ambient particle samples[29] and their role as photosensitizers have been studied in secondary organic aerosol formation.[30] Pyruvic acid has been found the atmospheric particles as well as at the sea surface microlayer.[31,32] Polydisperse particles with a number mode diameter of ∼80 nm were generated via atomization of a solution containing 10 g L^{-1} sodium nitrate (or ammonium nitrate, or sodium nitrate with added photosensitizers) with 2 g L^{-1} sodium sulfate dissolved in Milli-Q water. Sulfate was initially added to the solution as an internal standard to probe the loss of nitrate from particles, though later it was found that nitrate loss due to photolysis is too small to be detected by this approach (see Section 2.2). Experiments with and without sulfate were found to yield similar renoxification rate constants, suggesting that the presence of sulfate does not affect nitrate photolysis. Therefore, the nitrate/sulfate mixture was used throughout for experimental consistency. For experiments with ammonium nitrate, to minimize ammonium nitrate evaporation, the chamber was also filled with 50−100 ppm NH_3, by bubbling air through an ammonium hydroxide solution during the experiments.

The droplets from the atomizer were introduced into the chamber (without drying) for ∼2 min to reach the desired level of particle concentration (100−600 $\mu g\ m^{-3}$). Shortly after particle injection, UV lights were turned on to initiate photolysis, and experiments lasted for 20 min. After every experiment, the chamber walls were cleaned with deionized water and then dried by flushing the chamber with ultra-zero air to remove any particles or gases that had collected on the chamber walls.

A suite of particle- and gas-phase instruments (summarized in Table S1 and described in detail in the Supporting Information) sampled from the chamber to measure nitrogen-containing species. Gas-phase measurements included NO and NO_2 by a NO_{xy} analyzer (Air Quality Design Inc., described below) and HONO and HNO_3 by an iodide chemical ionization mass spectrometer (I-CIMS, Aerodyne Research Inc.) or by ion chromatography (Thermo Fisher) coupled with gas-phase denuders. Detailed descriptions of the I-CIMS calibration and denuder measurements are given in Sections 2.2 and 2.3 in the Supporting Information. In some experiments, HONO and HNO_3 measurements were not available, so we used a 0-D model to constrain the possible levels of HONO and HNO_3 in the total produced N from

https://dx.doi.org/10.1021/acs.est.0c06049
Environ. Sci. Technol. 2021, 55, 854−861

photolysis (more details in Section 2.4). An aerosol mass spectrometer (Aerodyne Research Inc.) and a scanning mobility particle sizer (TSI Inc.) were used to measure the concentration of nitrate particles. Other measurements included O_3 (2B Tech), temperature, and relative humidity (TE Connectivity). More information about the instruments is presented in the Supporting Information.

The central instrument in this study is the NO_{xy} analyzer, a dual-channel chemiluminescence instrument (built by Air Quality Design Inc.) operated at a measurement frequency of 1 Hz.[33] NO_x was detected by channel 1 using a blue light converter (BLC) and NO was detected by channel 2. NO_2 was derived by subtracting NO from NO_x. The BLC photolytically converts NO_2 to NO over a narrow wavelength band (395 nm), thus providing a selective measurement. The sensitivity of the instrument and the conversion efficiencies of the converters (BLC and Mo) were calibrated at the beginning of every experiment using a certified reference mixture of NO in N_2 (Airgas). A summary of instrument sensitivity and converters' conversion efficiencies at different relative humidities (RH) is shown in Figure S2. The instrument background (tested by flowing O_3 to pre-reactors for 30 s to react with the sample flow before it reached the detector) was subtracted from the measurement signal to calculate the mixing ratio. The detection limits of NO, NO_2, NO_x, and NO_y were 41, 68, 52, and 48 ppt s^{-1}, respectively (Figure S3).

2.2. Renoxification Rate Constant Determination. The primary objective of this work is to determine the renoxification rate constant from nitrate aerosol ($j_{pNO_3^-}$). This is the total rate constant for nitrate decay and product formation, and is distinct from the rate constants of the elementary reactions occurring within the particle. While nitrate photolysis is known to produce NO_2 and HONO directly, secondary gas-phase chemistry in the chamber can redistribute the photolysis products, primarily via the following reactions:

$$NO_2 + h\nu \rightarrow NO + O \quad (R3)$$

$$NO_2 + OH \rightarrow HNO_3 \quad (R4)$$

$$NO + OH \rightarrow HONO \quad (R5)$$

$$HONO + h\nu \rightarrow NO + OH \quad (R6)$$

Therefore, the calculation of the renoxification rate constant ($j_{pNO_3^-}$) includes the summed mass production (P) of gaseous NO, NO_2, HONO, and HNO_3, all of which have been corrected for dilution:

$$j_{pNO_3^-} = \frac{P_{NO} + P_{NO_2} + P_{HNO_3} + P_{HONO}}{\text{time} \times pNO_{3\,\text{total}}^-} \quad (E2)$$

where time is the duration of UV irradiation. In-particle concentrations of NO, NO_2, and HONO were extremely small given the low Henry's law constants.[34] The in-particle concentration of nitrite ions was determined to be negligible as well and was found not to accumulate in the particles (more details in the Supporting Information). $pNO_3^-{}_{\text{total}}$ is the mass concentration of particulate nitrate (in $\mu g\ m^{-3}$), which includes both suspended particles ($pNO_{3\,\text{suspended}}^-$) and particles lost to the chamber wall ($pNO_{3\,\text{wall}}^-$):

$$pNO_{3\,\text{total}}^- = pNO_{3\,\text{suspended}}^- + pNO_{3\,\text{wall}}^- \quad (E3)$$

All mass concentrations are converted to mass concentration of N for $j_{pNO_3^-}$ calculation. The change in $pNO_{3\,\text{total}}^-$ is controlled by two processes: chemical loss due to photolysis and loss of $pNO_{3\,\text{suspended}}^-$ due to chamber dilution. Chemical loss was found to be negligible since the total production of gas-phase products (on the order of 1 $\mu g\ m^{-3}$) is much smaller than the particle mass (hundreds of $\mu g\ m^{-3}$), so we treat chemical loss from the particles as negligible. The wall loss rate of $pNO_{3\,\text{suspended}}^-$ is faster than dilution loss, meaning that suspended nitrate mostly ends up on the chamber walls instead of being lost to chamber dilution. Thus, $pNO_{3\,\text{total}}^-$ did not change significantly during an experiment (see Section 3.1). One single value for $pNO_{3\,\text{total}}^-$ was adopted, which was the average concentration of $pNO_{3\,\text{total}}^-$ across each experiment. In addition, as discussed in Section 3.1, no differences in NO_x production between suspended and deposited nitrate particles were observed across a range of RH conditions, suggesting that $pNO_{3\,\text{suspended}}^-$ and $pNO_{3\,\text{wall}}^-$ have similar photolysis rate constants. Therefore, we did not attempt to treat them separately when calculating renoxification (eq E2). For consistency with previous studies,[16,18,21] our final results of the renoxification of particulate nitrate are presented as enhancement factors (eq E1).

2.3. Characterization of Chamber Lights. Enhancement factors rely on values of j_{HNO_3}, which was determined from measured chamber lamp output. Depending on the experiment, either 18 UVA lights (maximum irradiance at 340 nm) or 18 UVB lights (maximum irradiance at 313 nm) were used to illuminate the chamber to explore the wavelength dependence of nitrate photolysis. Figure 1 shows the total photon intensity inside the chamber under UVA and UVB conditions. The spectrum of the UVA lights has a good overlap with the solar spectrum at a 0° solar zenith angle.[7] The wavelength-dependent effective irradiances ($I_{\text{irradiance}}(\lambda)$) inside the chamber were measured for UVA and UVB by combining two approaches, a spectrometer-based measurement to determine the output light spectrum, and an actinometry-based measurement to infer the overall integrated photon flux. First, the wavelength-dependent light output

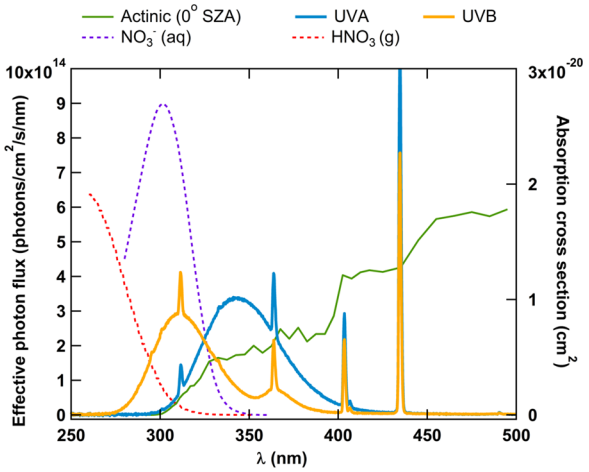

Figure 1. Wavelength dependences of UV light sources and nitrate absorption cross sections.[2,35] Solid curves: spectra of chamber lights and solar radiation[7] (at a 0° solar zenith angle). Dashed curves: absorption cross section of aqueous nitrate[2] (NO_3^-(aq)) and gas-phase nitric acid[35] (HNO_3(g)).

https://dx.doi.org/10.1021/acs.est.0c06049
Environ. Sci. Technol. 2021, 55, 854−861

($I_{\text{spectrometer}}(\lambda)$) was measured by a spectrometer (Ocean Optics, 200−850 nm, 1.5 nm FWHM optical resolution) by inserting the spectrometer probe into the center of the chamber. The probe contained a 600 μm fiber and a cosine corrector that collected signals from a 180° field of view. The spectrometer measurements enabled the determination of the shape of the irradiance spectrum and the integrated photolysis rate ($j_{NO_2,\text{ spectrometer}}$) at that single location. However, the absolute accuracy of the spectrometer is unknown, introducing a potential source or error in the measurement. Thus, NO_2 actinometry was used to determine the absolute effective NO_2 photolysis rate ($j_{NO_2,\text{ actinometry}}$); determination of $j_{NO_2,\text{ measured}}$ is described in the Supporting Information. This value is then used to scale $I_{\text{spectrometer}}$ to determine $I_{\text{effective}}$:

$$I_{\text{effective}}(\lambda) = I_{\text{spectrometer}}(\lambda) \times \frac{j_{NO_2,\text{ actinometry}}}{j_{NO_2,\text{ spectrometer}}} \quad \text{(E4)}$$

The heterogeneity of photon flux in different locations inside the chamber and the fluctuation of the irradiance from the lights were also investigated and were found to be negligible (Figures S4 and S5). The absorbance spectra of gas-phase HNO_3[35] and aqueous nitrate[2] are also shown in Figure 1. The total j_{HNO_3} under UVA and UVB conditions were calculated using cross section and quantum yields from the literature,[35] and were applied in eq E1 to calculate enhancement factors.

2.4. Box Model Simulations. To better understand and constrain the redistribution of photolysis products in our chamber, a series of model simulations using a box model, Framework for 0-D Atmospheric Modeling (F0AM[36]), were performed to estimate the possible levels of HONO and HNO_3 in the total produced N from photolysis when HONO and HNO_3 measurements were not available. Reactions included in the box model and the simulation results are summarized in the Supporting Information. The model takes into account the initial conditions and photon intensity of the chamber. Simulations were performed only for the periods when the chamber was filled with particulate nitrate and the lights were on, with a total time of 1200 s. We ran scenarios for a variety of molar yield ratios of the photolysis products (NO_2, HONO, and NO), keeping the total renoxification rate constant the same across all scenarios.

3. RESULTS AND DISCUSSION

3.1. Renoxification from Particulate Sodium Nitrate. Figure 2 shows the time series of NO, NO_2, HONO, HNO_3, and pNO_3^- in a typical sodium nitrate photolysis experiment. The shadings denote the lights-on periods. The decay of $pNO_{3\text{ all}}^-$ in Figure 2a is from loss by dilution, which occurs independent of irradiation; as discussed in Section 2.2, chemical loss by photolysis is negligible for the particle loading in our experiments. The concentration of suspended particulate nitrate ($pNO_{3\text{ suspended}}^-$) is also plotted together with the total particulate nitrate ($pNO_{3\text{ total}}^-$) in the chamber.

After the particles were injected and lights were turned on, NO, NO_2, and HONO started to increase until the lights were turned off. The temperature change induced by turning on the UV lights was less than 1 °C within the period of our experiments, so negligible volatilization of $NaNO_3$ is expected. While most gas-phase species were formed only when nitrate particles were added and UV lights were turned on (Figure 2b), HONO was found to increase upon irradiation of a particle-free chamber (Figure 2c). This lights-on period before particle injection is used to determine the chamber background, interpreted as the production of HONO from impurities on the chamber wall. The impurities appear to be independent of particle addition since the chamber was cleaned. This production rate of HONO during the chamber background period was subtracted from the production rate when the chamber was filled with nitrate particles, to remove the influence of this additional source.

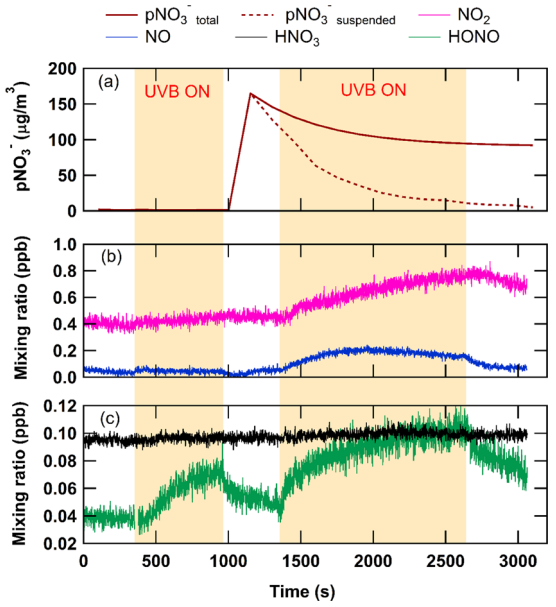

Figure 2. Time series of a typical particulate nitrate photolysis experiment. Areas in orange indicate periods with lights on. Time series for total particulate nitrate in the chamber ($pNO_{3\text{ total}}^-$), suspended particulate nitrate ($pNO_{3\text{ suspended}}^-$), NO and NO_2, and gaseous HONO and gaseous HNO_3 are shown in (a−c), respectively. Prior to injection of the particles, chamber lights were turned on for a short period to determine the renoxification from impurities on the chamber wall.

In all UVA and UVB experiments, little to no increase in gas-phase HNO_3 (potentially formed via R4) is observed by either the I-CIMS (Figure 2c) or denuder-IC measurements. As our box model suggests, the increase in HNO_3 under most simulations is much smaller than the increase in HONO or NO_x concentrations (Figure S9). Under UVA irradiation, the modeled increase in HNO_3 is minimal for any combination of product branching ratios. Under UVB irradiation, when NO_2 is the only photolysis product, the modeled increase in HNO_3 is similar to that of HONO, accounting for ∼15% of the total increase in the gas-phase nitrogen. While the lack of observed increase in HNO_3 suggests minimal HNO_3 formation, it instead might be due to loss to the sampling line or other surfaces before reaching the detector/collector, or it could be caused by the relatively high detection limit of the denuder (details in the Supporting Information). To account for this potential "missing" HNO_3 in the measurements, in our enhancement factor calculations, $[HNO_3] = [HONO]$ is applied as the upper bound for $[HNO_3]$, as suggested by the model simulations.

The major results from all $NaNO_3$ experiments are summarized in Figure 3, which gives the measured enhancement factors at different humidity levels under UVA and UVB conditions. The enhancement factor is close to zero (negligible

https://dx.doi.org/10.1021/acs.est.0c06049
Environ. Sci. Technol. 2021, 55, 854−861

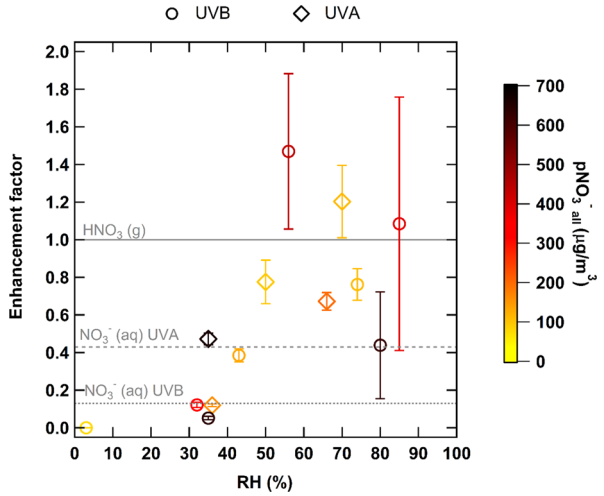

Figure 3. Enhancement factors for particulate sodium nitrate renoxification under UVA and UVB conditions at different values of relative humidity (RH). The solid gray line represents an enhancement factor of 1, indicating a particulate nitrate photolysis rate constant equal to that of gaseous HNO_3 at the same wavelength range. Data points are color coded by the particulate nitrate concentration ($pNO^-_{3\ total}$). Error bars represent the uncertainty propagated from the variability of the nitrate mass concentration in the chamber and the uncertainty in denuder-IC measurements. For reference, the enhancement factors of photolysis of aqueous NO_3^- under UVA and UVB, assuming 1% of quantum yield across all wavelengths are also plotted relative to j_{HNO_3} (dotted gray lines). A summary of all the experiment conducted is presented in Table S2.

renoxification) under dry conditions (3% RH) with larger values at elevated RH. The photolysis rate constant for UVA and UVB under high RH conditions are ~3×10^{-6} and ~2×10^{-5} s^{-1}, respectively. Due to the increase in gaseous HNO_3 photolysis in shorter wavelengths, the enhancement factors derived under humid conditions (RH > 30%) for both types of UV lights are similar, both in the range of 0.1−2 for RH > 30%. In contrast to the enhancement factors (>100) derived from the aerosol samples in some previous studies,[16,20,21] our results indicate that particulate $NaNO_3$ photolysis is not substantially faster than photolysis of gaseous HNO_3. The observed RH dependence may arise from two different effects. First, under dry conditions, particulate nitrate can be essentially solid,[37] and thus, the photolysis products cannot diffuse out of the particle but instead will recombine. Second, under high-RH conditions, nitrate particles should be aqueous, and the more dilute solute concentrations under high-RH may affect the wavelength dependence of the absorption of nitrate ions. Roca *et al.*[6] and Hudson *et al.*[38] found that at low solute concentrations, the absorption maximum (~302 nm) of nitrate solutions shifts slightly toward longer wavelengths, which would lead to absorption spectra that have stronger overlap with the irradiance spectra of the UV lights used here. Our present data do not allow us to distinguish the two effects, but both could be playing a role in the observed RH dependence.

For reference, the relative expected rate constants of nitrate photolysis in bulk aqueous solution under UVA and UVB relative to j_{HNO_3} are also shown in Figure 3. These use the cross sections shown in Figure 1 and assume a 1% quantum yield across all wavelengths. Our results thus indicate that renoxification from particulate nitrate is not substantially faster than that from aqueous nitrate. In addition, a strong dependence of renoxification rate constant on nitrate mass concentration was not observed (denoted by the colors in Figure 3). This is in contrast to the results of Ye *et al.*, who reported a logarithmic dependence on nitrate loading.[21]

When calculating the renoxification rate constant, it is assumed that suspended particles and particles lost to the chamber wall have a similar photolysis rate constant. This assumption was examined by running experiments in which particle photolysis was initiated after most of the injected particles had been lost to the wall (Figure S6). These results were compared with results from our standard experiments in which the photolysis was started shortly after the particle injection, when most of the particles were still suspended. The differences in enhancement factors are relatively small (Figure S7), suggesting that loss of particles to the chamber walls did not significantly affect our calculated renoxification rates. This is likely because particles deposited on the chamber wall were still within the chamber system and thus in the similar physical and chemical environment to the suspended particles during the period of the experiments.

3.2. Renoxification from Particulate Ammonium Nitrate. In addition to sodium nitrate, experiments with a similar setup under high RH conditions (50 and 70% RH) were conducted using ~300 $\mu g\ m^{-3}$ ammonium nitrate particles, and the results are compared with results from previous sodium nitrate particles under similar RH. NH_3 (50−100 ppm) was added to the chamber to minimize the volatilization of nitrate. The estimated particle pH in these experiments are in the range of 6.2−6.6 (the Extended Aerosol Inorganics Model, E-AIM[39−41]) with detailed estimation provided in the Supporting Information and Figure S8. Under this high NH_3(g) condition, results from E-AIM showed that more than 99% of the nitrate remained in the particle phase. Although this pH range is higher than that found in some regions, it is not unrealistic for atmospheric particles.[42] In this set of experiments, the HONO and HNO_3 measurements were not available, so we focus only on the production of NO_x. As Figure 4 shows, we find a factor of 2−3 increase in the NO_x production rate constant from particulate NH_4NO_3 (open diamonds) compared to $NaNO_3$ (open squares) under similar RH conditions. It is not clear why photolysis of NH_4NO_3 produced a higher level of NO_x; the branching ratios between R1 and R2 and the subsequent fate of any nitrite produced might depend on the water content, pH, and ionic strengths of the aqueous particles with two different cations.

To estimate the enhancement factors from particulate NH_4NO_3 photolysis, we used the F0AM box model to constrain the range of the possible HONO and HNO_3 contributions during the experiments compared to the measured NO_x contribution. As illustrated in Figure S9, when HONO is the only photolysis product, more than 70% of the increase in the total gaseous nitrogen budget will be HONO and HNO_3 in both UVA and UVB conditions. When NO and/or NO_2 are the only photolysis products, HONO and HNO_3 constitute less than 10% of the final products at the end of the simulation. Scaling the HONO and HNO_3 concentration from the NO_x concentration using the model simulations, the estimated enhancement factor for particulate NH_4NO_3 is [2.6, 8.4] for UVA and [0.5, 1.9] for UVB at 70% RH (the highest RH in the ammonium nitrate experiments).

3.3. Effects of Photosensitizers. Given that pure inorganic nitrate particles did not appear to contribute

https://dx.doi.org/10.1021/acs.est.0c06049
Environ. Sci. Technol. 2021, 55, 854−861

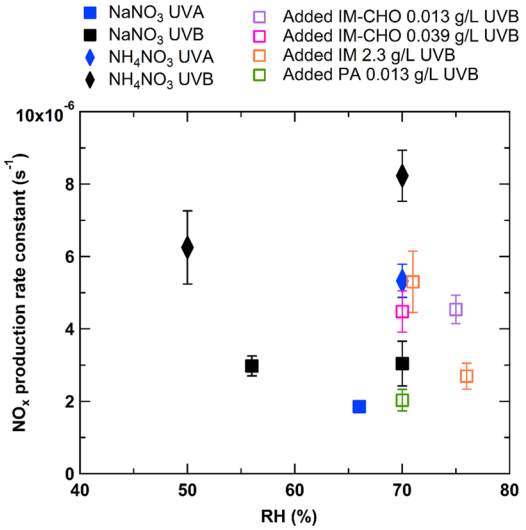

Figure 4. NO_x production rate constant for particulate NH_4NO_3 (solid diamonds), $NaNO_3$ without added photosensitizers (solid squares), and $NaNO_3$ with added photosensitizers (open squares). In general, under similar RH, the NO_x production rate constants for particulate NH_4NO_3 are about 2 times higher than particulate $NaNO_3$ There is no clear effect of photosensitizer addition. The concentrations of the photosensitizers are those of the atomization solution.

dramatically to renoxification, we also tested whether the presence of photosensitizers in particles might accelerate the renoxification process of particulate $NaNO_3$. Pyruvic acid (PA, 0.013 g L^{-1}), 2-imidazolecarboxaldehyde (IM-CHO, 0.013 g L^{-1} or 0.039 g L^{-1}), or imidazole (IM, 2.3 g L^{-1}) was added to the nitrate solution that was used to generate particulate nitrate. Experiments were conducted under high RH (70−76%) and UVB conditions to maximize the rate of NO_x and HONO production. Only NO_x measurements were available in these experiments, so we compare results only to the NO_x yields from non-sensitizer experiments. As Figure 4 shows, experiments with added IM-CHO show higher NO_x production, though the rate constants are within the same order of magnitude with experiments without the photosensitizers. Experiments with added PA and IM show no enhancement in producing NO_x within the uncertainty of the measurements. Since aqueous nitrate already absorbs at the UVB wavelengths (Figure 1), it is likely that adding photosensitizers will not have a large impact on photolysis. The effects under UV-A were not explored here and require additional study.

3.4. Implications and Future Work. In this study, we used two model systems, $NaNO_3$ and NH_4NO_3, to constrain the renoxification from particulate inorganic nitrate photolysis. We found that measured photolysis rate constant generally increases with increasing relative humidity, suggesting that the particle phase (solid vs deliquesced) is important in renoxification. Our derived enhancement factors are estimated to be <10 for inorganic nitrate particles under humid conditions. This range is much lower than the enhancement factor >100 suggested by some previous studies,[16,20,21] but is similar to the 1−30 range reported by Romer *et al.*[18] Using enhancement factors of 25−100, global model simulations from Kasibhatla *et al.* suggested peak relative enhancements ranging from factors of 5−20 for NO_x in the tropical and subtropical marine boundary layer.[19] To the extent that our systems are representative of inorganic nitrate particles in the real atmosphere, our results suggest that renoxification from the photolysis of inorganic particulate nitrate is not substantially faster than gaseous HNO_3 under UVA and UVB conditions. Such photolysis processes are therefore unlikely to have a dramatic impact on NO_x in remote environments.

In addition to the NO_x budget, photolysis of particulate nitrate may also affect the gas-phase OH budget, especially when HONO is the dominant photolysis product. Kasibhatla *et al.*[19] show that if an enhancement factor of 25 is applied to nitrate photolysis in coarse-mode sea salt particles, the OH concentration in the tropical and subtropical ocean will increase by 20% (using HONO:NO_2 molar yield of 0.67:0.33). The lower enhancement factors derived in this work therefore imply that the impact of particulate nitrate photolysis on the marine boundary layer OH is modest at best (<20%).

Our studies focus only on a few simple nitrate particle types, while ambient nitrate particles are more complex mixtures, involving a range of aerosol pH, water content, cation species, organic compounds (which may serve as OH scavengers), and halogen species. These properties can possibly affect aerosol nitrate photolysis,[3,5,6,43,44] but the magnitudes of the individual and the combined effects of these are unclear. In addition, we quantified only the production of NO_x and HONO in the gas phase, while some studies suggested that nitrate photochemistry can produce reduced nitrogen species such as N_2O as well as NO^- and N^- in the condensed phase.[12,45] Further, renoxification from organic nitrate photochemistry is even less understood and also warrants further investigation.[46,47] Thus, direct extrapolation of our results to ambient conditions should be done with caution. However, our experiments represent a starting point for investigating renoxification from suspended nitrate particles, indicating that inorganic nitrate particles ($NaNO_3$ and NH_4NO_3) do not contribute substantially to renoxification processes. Additional studies of more complex chemical systems, such as those described above, are needed.

■ ASSOCIATED CONTENT

Supporting Information

The Supporting Information is available free of charge at https://pubs.acs.org/doi/10.1021/acs.est.0c06049.

Determination of j_{NO_2}, instrument details, determination of particulate nitrate concentration in the chamber, in-particle nitrite ion concentration, box model details and simulation results, and particle pH estimation (PDF)

■ AUTHOR INFORMATION

Corresponding Author

Qing Ye − *Department of Civil and Environmental Engineering, Massachusetts Institute of Technology, Cambridge, Massachusetts 02139, United States;* orcid.org/0000-0003-3797-8988; Email: qye@mit.edu

Authors

Qianwen Shi − *Department of Physical and Environmental Sciences, University of Toronto Scarborough, Toronto, Ontario M1C 1A4, Canada*

Ye Tao − *Department of Physical and Environmental Sciences, University of Toronto Scarborough, Toronto, Ontario M1C 1A4, Canada;* orcid.org/0000-0003-1043-6687

https://dx.doi.org/10.1021/acs.est.0c06049
Environ. Sci. Technol. 2021, 55, 854−861

Jordan E. Krechmer − *Center for Aerosol and Cloud Chemistry, Aerodyne Research Incorporated, Billerica, Massachusetts 01821, United States*
Colette L. Heald − *Department of Civil and Environmental Engineering, Massachusetts Institute of Technology, Cambridge, Massachusetts 02139, United States;* orcid.org/0000-0003-2894-5738
Jennifer G. Murphy − *Department of Chemistry, University of Toronto, Toronto, Ontario M5S 3H6, Canada;* orcid.org/0000-0001-8865-5463
Jesse H. Kroll − *Department of Civil and Environmental Engineering, Massachusetts Institute of Technology, Cambridge, Massachusetts 02139, United States;* orcid.org/0000-0002-6275-521X

Complete contact information is available at: https://pubs.acs.org/10.1021/acs.est.0c06049

Notes

The authors declare no competing financial interest.

■ ACKNOWLEDGMENTS

This work is supported by the NOAA AC4 Program under grants NA18OAR4310110 and NA18OAR4310111. We also thank Dr. Amy Hrdina for her help with the IC measurements and Prof. Rachel O'Brien at College of William and Mary for her help with the spectrometer measurements.

■ REFERENCES

(1) Zhang, Q.; Jimenez, J. L.; Canagaratna, M. R.; Allan, J. D.; Coe, H.; Ulbrich, I.; Alfarra, M. R.; Takami, A.; Middlebrook, A. M.; Sun, Y. L.; Dzepina, K.; Dunlea, E.; Docherty, K.; DeCarlo, P. F.; Salcedo, D.; Onasch, T.; Jayne, J. T.; Miyoshi, T.; Shimono, A.; Hatakeyama, S.; Takegawa, N.; Kondo, Y.; Schneider, J.; Drewnick, F.; Borrmann, S.; Weimer, S.; Demerjian, K.; Williams, P.; Bower, K.; Bahreini, R.; Cottrell, L.; Griffin, R. J.; Rautiainen, J.; Sun, J. Y.; Zhang, Y. M.; Worsnop, D. R. Ubiquity and Dominance of Oxygenated Species in Organic Aerosols in Anthropogenically-Influenced Northern Hemisphere Midlatitudes. *Geophys. Res. Lett.* **2007**, *34*, 1−6.
(2) Blaszczak-Boxe, C. S.; Saiz-Lopez, A. Nitrate Photolysis in Ice and Snow: A Critical Review of Its Multiphase Chemistry. *Atmos. Environ.* **2018**, *193*, 224−241.
(3) Chu, L.; Anastasio, C. Quantum Yields of Hydroxyl Radical and Nitrogen Dioxide from the Photolysis of Nitrate on Ice. *J. Phys. Chem. A* **2003**, *107*, 9594−9602.
(4) Zatko, M.; Geng, L.; Alexander, B.; Sofen, E.; Klein, K. The Impact of Snow Nitrate Photolysis on Boundary Layer Chemistry and the Recycling and Redistribution of Reactive Nitrogen across Antarctica and Greenland in a Global Chemical Transport Model. *Atmos. Chem. Phys.* **2016**, *16*, 2819−2842.
(5) Scharko, N. K.; Berke, A. E.; Raff, J. D. Release of Nitrous Acid and Nitrogen Dioxide from Nitrate Photolysis in Acidic Aqueous Solutions. *Environ. Sci. Technol.* **2014**, *48*, 11991−12001.
(6) Roca, M.; Zahardis, J.; Bone, J.; El-Maazawi, M.; Grassian, V. H. 310 nm Irradiation of Atmospherically Relevant Concentrated Aqueous Nitrate Solutions: Nitrite Production and Quantum Yields. *J. Phys. Chem. A* **2008**, *112*, 13275−13281.
(7) Finlayson-Pitts, B. J.; Pitts, J. N., Jr. *Chemistry of the Upper and Lower Atmosphere: Theory, Experiments, and Applications*; Elsevier: 1999.
(8) Benedict, K. B.; McFall, A. S.; Anastasio, C. Quantum Yield of Nitrite from the Photolysis of Aqueous Nitrate above 300 Nm. *Environ. Sci. Technol.* **2017**, *51*, 4387−4395.
(9) Zhu, C.; Xiang, B.; Chu, L. T.; Zhu, L. 308 nm Photolysis of Nitric Acid in the Gas Phase, on Aluminum Surfaces, and on Ice Films. *J. Phys. Chem. A* **2010**, *114*, 2561−2568.
(10) Ye, C.; Gao, H.; Zhang, N.; Zhou, X. Photolysis of Nitric Acid and Nitrate on Natural and Artificial Surfaces. *Environ. Sci. Technol.* **2016**, *50*, 3530−3536.
(11) Zhou, X.; Gao, H.; He, Y.; Huang, G.; Bertman, S. B.; Civerolo, K.; Schwab, J. Nitric Acid Photolysis on Surfaces in Low-NO_x Environments: Significant Atmospheric Implications. *Geophys. Res. Lett.* **2003**, *30*, 10−13.
(12) Schuttlefield, J.; Rubasinghege, G.; El-Maazawi, M.; Bone, J.; Grassian, V. H. Photochemistry of Adsorbed Nitrate. *J. Am. Chem. Soc.* **2008**, *130*, 12210−12211.
(13) Rubasinghege, G.; Grassian, V. H. Photochemistry of Adsorbed Nitrate on Aluminum Oxide Particle Surfaces. *J. Phys. Chem. A* **2009**, *113*, 7818−7825.
(14) Laufs, S.; Kleffmann, J. Investigations on HONO Formation from Photolysis of Adsorbed HNO_3 on Quartz Glass Surfaces. *Phys. Chem. Chem. Phys.* **2016**, *18*, 9616−9625.
(15) Baergen, A. M.; Donaldson, D. J. Photochemical Renoxification of Nitric Acid on Real Urban Grime. *Environ. Sci. Technol.* **2013**, *47*, 815−820.
(16) Ye, C.; Zhou, X.; Pu, D.; Stutz, J.; Festa, J.; Spolaor, M.; Tsai, C.; Cantrell, C.; Mauldin, R. L.; Campos, T.; Weinheimer, A.; Hornbrook, R. S.; Apel, E. C.; Guenther, A.; Kaser, L.; Yuan, B.; Karl, T.; Haggerty, J.; Hall, S.; Ullmann, K.; Smith, J. N.; Ortega, J.; Knote, C. Rapid Cycling of Reactive Nitrogen in the Marine Boundary Layer. *Nature* **2016**, *532*, 489−491.
(17) Reed, C.; Evans, M. J.; Crilley, L. R.; Bloss, W. J.; Sherwen, T.; Read, K. A.; Lee, J. D.; Carpenter, L. J. Evidence for Renoxification in the Tropical Marine Boundary Layer. *Atmos. Chem. Phys.* **2017**, *17*, 4081−4092.
(18) Romer, P. S.; Wooldridge, P. J.; Crounse, J. D.; Kim, M. J.; Wennberg, P. O.; Dibb, J. E.; Scheuer, E.; Blake, D. R.; Meinardi, S.; Brosius, A. L.; Thames, A. B.; Miller, D. O.; Brune, W. H.; Hall, S. R.; Ryerson, T. B.; Cohen, R. C. Constraints on Aerosol Nitrate Photolysis as a Potential Source of HONO and NO_x. *Environ. Sci. Technol.* **2018**, *52*, 13738−13746.
(19) Kasibhatla, P.; Sherwen, T.; Evans, M. J.; Carpenter, L. J.; Reed, C.; Alexander, B.; Chen, Q.; Sulprizio, M. P.; Lee, J. D.; Read, K. A.; Bloss, W.; Crilley, L. R.; Keene, W. C.; Pszenny, A. A. P.; Hodzic, A. Global Impact of Nitrate Photolysis in Sea-Salt Aerosol on NO_x, OH, and O_3 in the Marine Boundary Layer. *Atmos. Chem. Phys.* **2018**, *18*, 11185−11203.
(20) Bao, F.; Li, M.; Zhang, Y.; Chen, C.; Zhao, J. Photochemical Aging of Beijing Urban $PM_{2.5}$: HONO Production. *Environ. Sci. Technol.* **2018**, *52*, 6309−6316.
(21) Ye, C.; Zhang, N.; Gao, H.; Zhou, X. Photolysis of Particulate Nitrate as a Source of HONO and NO_x. *Environ. Sci. Technol.* **2017**, *51*, 6849−6856.
(22) Chen, Q.; Edebeli, J.; McNamara, S. M.; Kulju, K. D.; May, N. W.; Bertman, S. B.; Thanekar, S.; Fuentes, J. D.; Pratt, K. A. HONO, Particulate Nitrite, and Snow Nitrite at a Midlatitude Urban Site during Wintertime. *ACS Earth Space Chem.* **2019**, *3*, 811−822.
(23) Haskins, J. D.; Lopez-Hilfiker, F. D.; Lee, B. H.; Shah, V.; Wolfe, G. M.; DiGangi, J.; Fibiger, D.; McDuffie, E. E.; Veres, P.; Schroder, J. C.; Campuzano-Jost, P.; Day, D. A.; Jimenez, J. L.; Weinheimer, A.; Sparks, T.; Cohen, R. C.; Campos, T.; Sullivan, A.; Guo, H.; Weber, R.; Dibb, J.; Green, J.; Fiddler, M.; Bililign, S.; Jaeglé, L.; Brown, S. S.; Thornton, J. A. Anthropogenic Control Over Wintertime Oxidation of Atmospheric Pollutants. *Geophys. Res. Lett.* **2019**, *46*, 14826−14835.
(24) Gen, M.; Zhang, R.; Huang, D. D.; Li, Y.; Chan, C. K. Heterogeneous Oxidation of SO_2 in Sulfate Production during Nitrate Photolysis at 300 nm: Effect of pH, Relative Humidity, Irradiation Intensity, and the Presence of Organic Compounds. *Environ. Sci. Technol.* **2019**, *53*, 8757−8766.
(25) Gen, M.; Zhang, R.; Huang, D. D.; Li, Y.; Chan, C. K. Heterogeneous SO_2 Oxidation in Sulfate Formation by Photolysis of Particulate Nitrate. *Environ. Sci. Technol. Lett.* **2019**, *6*, 86−91.
(26) Zheng, H.; Song, S.; Sarwar, G.; Gen, M.; Wang, S.; Ding, D.; Chang, X.; Zhang, S.; Xing, J.; Sun, Y.; Ji, D.; Chan, C. K.; Gao, J.;

McElroy, M. B. Contribution of Particulate Nitrate Photolysis to Heterogeneous Sulfate Formation for Winter Haze in China. *Environ. Sci. Technol. Lett.* **2020**, 632.
(27) Benedict, K. B.; Anastasio, C. Quantum Yields of Nitrite (NO_2^-) from the Photolysis of Nitrate (NO_3^-) in Ice at 313 nm. *J. Phys. Chem. A* **2017**, *121*, 8474−8483.
(28) Lim, C. Y.; Hagan, D. H.; Coggon, M. M.; Koss, A. R.; Sekimoto, K.; de Gouw, J.; Warneke, C.; Cappa, C. D.; Kroll, J. H. Secondary Organic Aerosol Formation from the Laboratory Oxidation of Biomass Burning Emissions. *Atmos. Chem. Phys.* **2019**, *19*, 12797−12809.
(29) Teich, M.; van Pinxteren, D.; Kecorius, S.; Wang, Z.; Herrmann, H. First Quantification of Imidazoles in Ambient Aerosol Particles: Potential Photosensitizers, Brown Carbon Constituents, and Hazardous Components. *Environ. Sci. Technol.* **2016**, *50*, 1166−1173.
(30) Aregahegn, K. Z.; Nozière, B.; George, C. Organic Aerosol Formation Photo-Enhanced by the Formation of Secondary Photosensitizers in Aerosols. *Faraday Discuss.* **2013**, *165*, 123−134.
(31) Kawamura, K.; Yasui, O. Diurnal Changes in the Distribution of Dicarboxylic Acids, Ketocarboxylic Acids and Dicarbonyls in the Urban Tokyo Atmosphere. *Atmos. Environ.* **2005**, *39*, 1945−1960.
(32) Steinberg, S. M.; Bada, J. L. Oxalic, Glyoxalic and Pyruvic Acids in Eastern Pacific Ocean Waters. *J. Mar. Res.* **1984**, *42*, 697−708.
(33) Geddes, J. Observations of Reactive Nitrogen Oxides: From Ground Level Ozone Production to Biosphere-Atmosphere Exchange in Downwind Forest Environments. University of Toronto, 2014.
(34) Sander, R. Compilation of Henry's Law Constants (Version 4.0) for Water as Solvent. *Atmos. Chem. Phys.* **2015**, *15*, 4399−4981.
(35) IUPAC *Task Group on Atmospheric Chemical Kinetic Data Evaluation*. http://iupac.pole-ether.fr/
(36) Wolfe, G. M.; Marvin, M. R.; Roberts, S. J.; Travis, K. R.; Liao, J. The Framework for 0-D Atmospheric Modeling (F0AM) v3.1. *Geosci. Model Dev.* **2016**, *9*, 3309−3319.
(37) Gregson, F. K. A.; Robinson, J. F.; Miles, R. E. H.; Royall, C. P.; Reid, J. P. Drying and Crystallization of Evaporating Sodium Nitrate Aerosol Droplets. *J. Phys. Chem. B* **2020**, *124*, 6024−6036.
(38) Hudson, P. K.; Schwarz, J.; Baltrusaitis, J.; Gibson, E. R.; Grassian, V. H. A Spectroscopic Study of Atmospherically Relevant Concentrated Aqueous Nitrate Solutions. *J. Phys. Chem. A* **2007**, *111*, 544−548.
(39) Wexler, A. S.; Clegg, S. L. Atmospheric Aerosol Models for Systems Including the Ions H^+, NH_4^+, Na^+, SO_4^{2-}, NO_3^-, Cl^-, Br^-, and H_2O. *J. Geophys. Res.* **2002**, *107*, ACH-14.
(40) Clegg, S. L.; Brimblecombe, P.; Wexler, A. S. Thermodynamic Model of the System H^+−NH_4^+ −Na^+−SO_4^{2-}−NO_3^-−Cl^-−H_2O at 298.15 K. *J. Phys. .Chem. A* **1998**, *102*, 2155−2171.
(41) Clegg, S. L.; Pitzer, K. S.; Brimblecombe, P. Thermodynamics of Multicomponent, Miscible, Ionic Solutions. Mixtures Including Unsymmetrical Electrolytes. *J. Phys. Chem.* **1992**, *96*, 9470−9479.
(42) Xie, Y.; Wang, G.; Wang, X.; Chen, J.; Chen, Y.; Tang, G.; Wang, L.; Ge, S.; Xue, G.; Wang, Y.; Gao, J. Nitrate-Dominated $PM_{2.5}$ and Elevation of Particle pH Observed in Urban Beijing during the Winter of 2017. *Atmos. Chem. Phys.* **2020**, *20*, 5019−5033.
(43) Petriconi, G. L.; Gori, E. G.; Papée, H. M. Effect of Chloride Concentration on the Decomposition of Aqueous Sodium Nitrate by Sunlight. *Pure Appl. Geophys.* **1969**, *72*, 299−306.
(44) Yang, W.; Han, C.; Yang, H.; Xue, X. Significant HONO Formation by the Photolysis of Nitrates in the Presence of Humic Acids. *Environ. Pollut.* **2018**, *243*, 679−686.
(45) Nanayakkara, C. E.; Jayaweera, P. M.; Rubasinghege, G.; Baltrusaitis, J.; Grassian, V. H. Surface Photochemistry of Adsorbed Nitrate: The Role of Adsorbed Water in the Formation of Reduced Nitrogen Species on α-Fe_2O_3 Particle Surfaces. *J. Phys. Chem. A* **2014**, *118*, 158−166.
(46) Nah, T.; Sanchez, J.; Boyd, C. M.; Ng, N. L. Photochemical Aging of α-Pinene and β-Pinene Secondary Organic Aerosol Formed from Nitrate Radical Oxidation. *Environ. Sci. Technol.* **2016**, *50*, 222−231.
(47) Müller, J. F.; Peeters, J.; Stavrakou, T. Fast Photolysis of Carbonyl Nitrates from Isoprene. *Atmos. Chem. Phys.* **2014**, *14*, 2497−2508.

https://dx.doi.org/10.1021/acs.est.0c06049
Environ. Sci. Technol. 2021, 55, 854−861